

Article

Characterization of Materials Used in the Concrete Industry, from the Point of View of Corrosion Behavior

Marius Gabriel Petrescu , Razvan George Ripeanu , Eugen Laudacescu , Maria Tanase , Adrian Niță and Andrei Burlacu

Mechanical Engineering Department, Petroleum-Gas University of Ploiești, 100680 Ploiești, Romania; pmarius@upg-ploiesti.ro (M.G.P.); rrapeanu@upg-ploiesti.ro (R.G.R.); leugen@upg-ploiesti.ro (E.L.); nita_adrian007@yahoo.com (A.N.); andreiburlacu1987@gmail.com (A.B.)

* Correspondence: maria.tanase@upg-ploiesti.ro

Abstract: Industrial applications in the concrete industry face significant challenges in selecting appropriate metallic materials, as these choices can enhance equipment lifespan and reduce costs. This study examines the corrosion behavior of various metallic materials, offering valuable insights for their selection in corrosive environments. The findings indicate that material testing can provide cost-effective solutions for concrete industry equipment. Notably, replacing cast iron used in concrete mixing blades with specific steels is advantageous for corrective or accidental maintenance, lowering spare parts costs, and short-term use, steels P265GH and AISI 4140 exhibiting corrosion resistance similar to cast iron. Additionally, for mineral aggregate dryers, selecting adequate steel can significantly reduce operating and maintenance costs while increasing equipment durability. The results show that substituting steel S235 with steel P265GH can decrease the corrosion rate by nearly 65%.

Keywords: corrosion rate; steel; cast iron; electrochemical properties; concrete industry



Citation: Petrescu, M.G.; Ripeanu, R.G.; Laudacescu, E.; Tanase, M.; Niță, A.; Burlacu, A. Characterization of Materials Used in the Concrete Industry, from the Point of View of Corrosion Behavior. *Coatings* **2024**, *14*, 800. <https://doi.org/10.3390/coatings14070800>

Academic Editors: Peng Liu and Lingkun Chen

Received: 23 May 2024

Revised: 19 June 2024

Accepted: 24 June 2024

Published: 27 June 2024



Copyright: © 2024 by the authors. Licensee MDPI, Basel, Switzerland. This article is an open access article distributed under the terms and conditions of the Creative Commons Attribution (CC BY) license (<https://creativecommons.org/licenses/by/4.0/>).

1. Introduction

The equipment utilized in large-scale concrete production is designed to withstand significant operational stresses, primarily arising from the abrasive impact of mineral aggregates (such as sand and variously sized stones) and the corrosive effects of the water-cement dust blend [1]. In the realm of the concrete industry, where efficiency, reliability, and durability are paramount, corrosion is posing significant challenges to the integrity and performance of essential equipment such as rotary dryers and concrete mixers. These industrial equipment, vital for the production and processing of materials from the concrete composition, confronts corrosion-induced degradation that compromises operational efficiency and safety.

Rotary dryers, revered for their efficiency in drying mineral aggregates, and concrete mixers, indispensable for homogenizing concrete mixtures, both struggle with corrosion-induced deterioration that compromises their functionality and longevity. Understanding the nuanced interplay between corrosion and materials within these equipment types is essential for devising prevention measures.

The flight assembly of rotary dryers, serving in material transport and heat transfer [2], faces corrosive attack from moisture, abrasive particles, and chemical contaminants inherent in mineral aggregates. Conversely, the mixing blades of concrete mixers, tasked with blending cement, aggregates, water, and additives, endure corrosive exposure to alkaline environments, chloride ingress, carbonation, and aggressive chemicals present in concrete mixtures.

At the base of corrosion lies an electrochemical process wherein metallic surfaces interact with their environment, initiating chemical reactions determining the degradation of material over time. In both rotary dryers and concrete mixers, this process is compounded

by intrinsic factors such as material composition, design intricacies, and operational parameters, as well as extrinsic factors including environmental conditions, maintenance practices, and exposure duration.

In case of rotary dryer, many studies [3–8] concentrated on identifying the factors that influence their performance of rotary dryers, by reference to the distribution of the particles inside the drum. Only the study [1] investigated the tribological behavior of materials used in rotary dryer blades, focusing on abrasive and abrasive-erosive wear, using the Baroid tester. The results identified abrasive erosion as the primary cause of blade damage and outlined the conditions that exacerbate specific wear phenomena.

In case of concrete mixers, some studies [9–11] analyzed stress states in the arms and blades of mixers, using these stress states as key indicators to evaluate abrasive wear caused by impact and friction with aggregates. The wear characteristics of concrete mixers resistance was investigated in the referenced literature [12–16]. The study [17] focused on the concrete industry, comparing the abrasion-corrosion resistance of A36 carbon steel, advanced high-strength steels (AHSSs), and ASTM 410 ferritic stainless steels. Laboratory and field tests, including rubber wheel and microabrasion tests, were conducted using adapted concrete mixers and actual mixing equipment. Analysis revealed that ferritic stainless steel, despite lower hardness, outperformed AHSSs and significantly extended equipment lifespan.

In the previous work of the authors [16], three types of chromium-alloyed cast iron were tested under accelerated wear conditions simulating a real working environment (mix of mineral aggregate, sand, cement, and water) using a Baroid tribometer. The tests revealed that cast iron with the highest chromium content showed the best wear resistance overall. However, the study found that wear resistance did not consistently increase with chromium content. Specifically, cast iron with around 4% chromium performed better than those with about 9% chromium when the chromium content was below 25%. The investigation was extended in the paper [18] where the same types of chromium-alloyed cast irons used in mixing blades were used, focusing on their wear resistance in a working environment of crushed mineral aggregates (4–8 mm), using a special designed experimental stand that replicated a half-scale double-axis horizontal mixer that allowed for adjustment of the mixing blade attack angles to 30, 45, and 60 degrees. The results demonstrated a correlation between the blade material type and wear rate and showed that increasing the blade's inclination angle relative to the shaft axis significantly reduced cumulative mass loss by 43% to 55.83%, depending on the blade material quality.

Analyzing the existent literature in the field, can be find many works related to the corrosion analysis of different materials in concrete environment [19–35]. The laboratory study [19] assessed the corrosion activity of reinforcing steel in ordinary and high-performance concrete using various measurement methods. The findings revealed that Tafel plot, linear polarization resistance, half-cell potential, and chloride content methods predicted the same corrosion activity level for only 24% of the specimens.

Garcia et al. [20] investigated how embedded steel reinforcement corrodes under anoxic conditions with varying chloride concentrations. Three electrochemical techniques were used to measure corrosion rates: linear polarization resistance, electrochemical impedance spectroscopy, and chronopotentiometry. The maximum observed current density was $0.98 \mu\text{A}/\text{cm}^2$, regardless of chloride content. Using an Evans diagram, researchers estimated the cathodic Tafel constant to be 180 mV dec^{-1} , with a limit current density of $0.98 \mu\text{A}/\text{cm}^2$. The corrosion potential likely ranged from $-900 \text{ mVAg}/\text{AgCl}$ to $-1000 \text{ mVAg}/\text{AgCl}$, with the most probable corrosion current density between $0.22 \mu\text{A}/\text{cm}^2$ and $0.61 \mu\text{A}/\text{cm}^2$. The rapid galvanostatic pulse technique was implemented [21] on-site across numerous measurement points, covering a spectrum of reinforcement conditions from severe corrosion to passivity.

Field investigations were conducted in [36] to assess the corrosion of reinforcements in underground metro tunnels built between 1980 and 2006. On-site measurements included carbonation depth, half-cell potential, and concrete resistivity, while the chloride profile

of cored concrete specimens was analyzed in the laboratory. The analysis revealed the relationship between corrosion potential (half-cell potential) and corrosion rate. The study also examined the impact of galvanic coupling on localized and macrocell corrosion. The findings showed that a drop in half-cell potential near NaCl crystallization indicates chloride-induced corrosion.

The present study presents a thorough investigation into electrochemical parameters influencing corrosion behaviors in materials widely used in the concrete industry, focusing on rotary dryers (Figure 1a) and concrete mixers (Figure 1b). By examining polarization curves and Tafel plots from tests on cast iron and steel specimens, the research uncovers unexpected findings. The research offers practical implications for selecting corrosion-resistant materials for equipment like rotary dryers and concrete mixers. Certain steel samples, designated as suitable for mixer equipment, and others recommended for dryers, show promise in withstanding corrosive environments. Overall, the findings provide strategic recommendations for optimizing equipment durability and performance in the concrete industry, highlighting the essential role of electrochemical analysis in addressing corrosion phenomena.

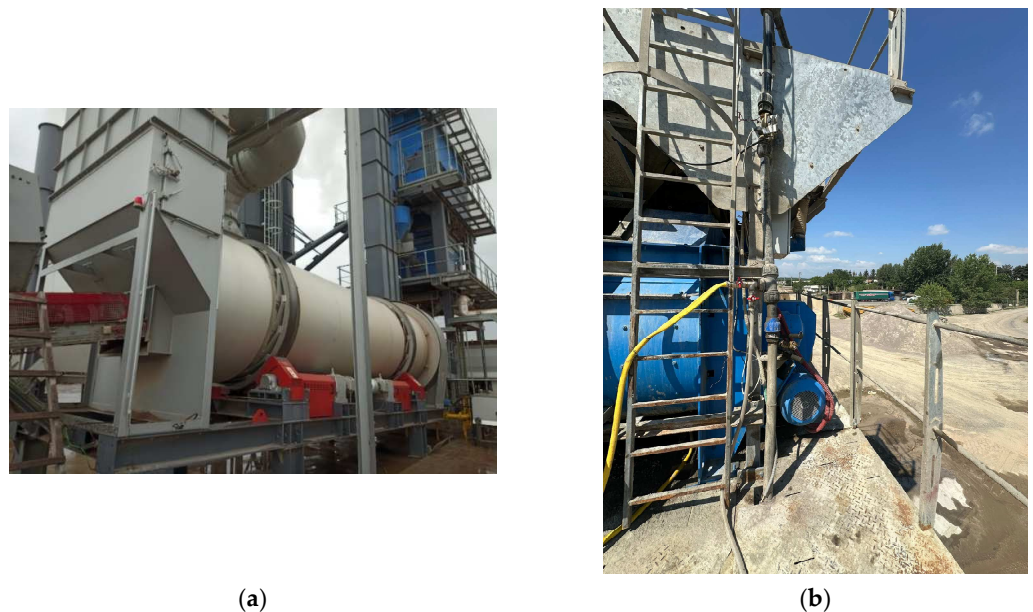


Figure 1. Concrete industry equipment: (a) rotary dryer; (b) concrete mixer.

2. Materials and Methods

2.1. Equipment Used for the Electrochemical Corrosion Testing

In order to perform the tests to determine the parameters characterizing the corrosion behavior of commonly used materials, a VoltaLab (Tacussel-Radiometer PGZ 100, Hatch Company, Mississauga, ON, Canada) potentiostat was used and the software was VoltaMaster 4.

To determine the electrochemical parameters of the tested materials, the Tafel technique was chosen, which focuses on the problems that accurately determine the corrosion rate of the material. With this technique, a controlled scanned potential is applied to the specimen, starting at an assumed corrosion potential, and then being extended in both anodic and cathodic directions by several hundred millivolts.

It should be noted that the “polarization resistance” technique is even faster than the Tafel technique, sometimes being complementary to it, due to the much smaller scanned area. Corrosion cell (Figure 2) works with a saturated calomel reference electrode and specimen holder exposes 1 cm^2 of the specimen to the test solution. Electrochemical tests were made according to ASTM G5-94 [37], and ASTM G1-90 [38].

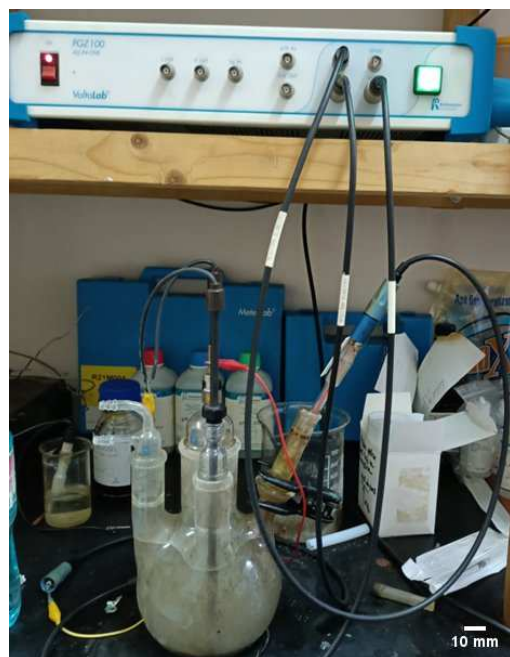


Figure 2. Corrosion cell.

When beginning the work sequence, the analysis technique is selected, and the parameters for the test cell are set. These parameters include the potential of the calomel reference electrode, its surface area, the surface area of the counter-graphite electrodes, and the surface area of the working electrode, which is 1 cm^2 . Additionally, the atomic mass of iron (Fe) is considered to be 55.85, and the ion valence is set to 2. The potential sweep range is defined from -1 V to $+1 \text{ V}$, with possible limits extending from -3 V to $+3 \text{ V}$, and the sweep rate is set to 1 mV/s .

2.2. Sample Selection and Preparation

The disk samples used for the test were taken from sheet-type semi-finished products, in the case of steels, and cast solids, in the case of cast irons.

The selection of cast iron and steel types was made based on experience in concrete manufacturing plants (cement concrete and asphalt concrete) considering the place of use and the working environment [1,18]. The selected cast irons are specific to the mixing blade materials of concrete mixers. Also, some of the selected steels were proposed to replace—within the maintenance interventions—the cast irons when making the mixing blades of the mixers. The use of steels instead of cast irons can be justified by the lower price of materials and the accessible technology of obtaining semi-finished products. Several types of steels have been selected for specific applications of dryers (with rotary drum) in asphalt concrete production plants. Tables 1 and 2 present the chemical composition and the corresponding microstructure of cast irons samples, and in Table 3 is indicated the chemical composition of steel samples. The three types of cast iron and steels proposed for use in concrete mixers were tested in aqueous cement environment (cement paste, Table 4) and steels with applications in rotary dryers were tested in water (Table 4).

Table 1. The chemical composition of the cast iron samples [18].

Sample	Chemical Composition, wt.%								
	C	Si	P	S	Cr	Mn	Fe	Ni	Mo
F1	3.28	0.76	0.07	0.03	3.83	1.10	89.86	0.89	0.20
F2	3.72	0.74	0.02	0.04	25.65	0.87	68.19	0.040	0.35
F3	3.08	0.96	0.04	0.03	9.77	1.14	84.12	0.35	0.49

Table 2. The microstructures and hardness values for the cast iron samples [16].


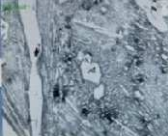

Sample	Sample Microstructure	Hardness HV0.2 (Average of Three Measurements)		Occupied Surface by the Hard Constituents, %	Hardness HV0.2, (Weighted Average)
		Matrix	Carbide		
1	 Low cast iron alloyed with Cr (4%), pearlite, ledeburites, and secondary cementites	318	644	44.986	464.654
2	 High cast iron alloyed with Cr (25%), austenitic structure with carbides	718	1632	55.854	1228.505
3	 Medium cast iron alloyed with Cr (9%), pearlite, secondary cementite, and ledeburite	462	799	50.739	632.990

Table 3. Chemical composition of steel samples.

Steel	Chemical Composition, wt. %															
	Fe	C	Si	Mn	P	S	Cr	Mo	Ni	Al	Co	Cu	Nb	Ti	V	W
A P355GH: EN10028 [39] (ASME SA 516 GRADE 70 [40])	97.384	0.264	0.175	1.229	0.013	0.005	0.362	0.040	0.181	0.020	0.010	0.256	0.002	0.044	0.005	0.010
B X5CrNi18-10 (1.4301): EN 10088 [41] (AISI 304)	72.151	0.08	0.110	1.260	0.006	0.003	18.010	0.020	8.030	-	0.130	0.090	0.010	0.090	0.010	-
B' P265GH (1.0425): EN 10028 [39]	98.659	0.072	0.098	0.51	0.007	0.004	0.12	0.03	0.09	-	0.14	0.08	0.01	0.12	0.06	-
C (AISI 4140 ASTM A29 [42]/42Cr4Mo2 EN 10083 [43]; rolled semi-finished product, thickness $s = 4$ mm)	98.291	0.289	0.252	0.468	0.011	0.003	0.340	0.020	0.030	0.035	0.007	0.026	0.040	0.110	0.058	0.020
D AISI 4140 ASTM A29 [42]/42Cr4Mo2 EN 10083 [43]; rolled semi-finished product, thickness $s = 3$ mm)	97.775	0.174	0.034	1.390	0.010	0.003	0.07	0.0017	0.06	0.021	-	0.23	0.0004	0.14	0.09	-
E (S275 EN 10025 [44]; laminated semi-finished product, thickness $s = 2$ mm)	98.721	0.075	0.004	0.268	0.021	0.011	0.170	0.040	0.130	-	0.100	-	-	0.380	0.050	0.030
F (S185 EN 10025 [44]; laminated semi-finished product, thickness $s = 2$ mm)	98.403	0.051	0.005	0.300	0.018	0.013	0.200	0.060	0.270	-	0.340	-	-	0.220	0.110	0.010
G G (S355 JR SR EN 10025 [44] laminated semi-finished product, thickness $s = 4$ mm)	98.390	0.090	0.040	0.760	0.014	0.011	0.130	0.040	0.140	0.015	0.100	0.100	0.010	0.050	0.100	0.010
S-flight material (S235 EN 10025 [44]; Rolled semi-finished products, thickness $s = 4$ mm)	98.380	0.1710	0.0320	1.370	0.0106	0.0032	0.0279	0.0017	0.00205	-	-	-	0.0005	-	0.0029	-

Table 4. The environments used for testing the steel samples.

Steel Sample	A	B	B'	C	D	E	F	G	S
Environment	Cement paste	Cement paste/water	Cement paste/water	Cement paste	Water	Water	Water/Cement paste	water	water

The results of the microstructure analysis for the three types of materials and the hardness measurements can be seen in Table 2. The microstructure of the three samples is specific to white hypoeutectic cast irons, presenting hard constituents in different forms, depending on the Cr content.

The chemical composition was determined using Genius 5000 X-ray Fluorescence Spectrometer (Skyray Instruments, Dallas, Texas, USA) using Positive Material Identification (PMI) principle.

It was also tested in the working environment (water), the steel (denoted as S) from the flights of rotary dryer used to dry the mineral aggregates, as seen in Figure 3.

**Figure 3.** The flights of rotary dryer.

The testing environment had the following characteristics:

A cement paste mixture composed of cement dust and water in a ratio of approximately 1 part cement dust to 2.75 parts water.

The density of this mixture, as measured in the laboratory, was about 1170 kg/m³.

The use of cement paste was intended to prevent solidification during the testing process.

The average pH of the mixture was 11.84, at the ambient temperature of 25.5 °C. The water used had a pH of 7.54.

The tests were conducted in the resulting aqueous solution after the coarse components had settled out. Therefore, the tests were performed in an environment with the described characteristics (pH 11.84, temperature 25.5 °C).

The samples were mechanically processed in the form of discs with 16 mm diameter and 2~4 mm thickness.

The mechanical processing was carried out with low cutting rates using cooling liquids, in order not to introduce mechanical or thermal stresses in the processed material and thereby maintain the structure and initial physico-chemical qualities of the materials.

One of the surfaces of the disc samples, the one that will come into contact with the work environment, was sanded wet on abrasive paper, initially with the 250 Mesh grit size and then with the 600 Mesh grit size.

Before the specimens were mounted in the fixture for testing, they were placed in boiling benzene for 5 min. Specimens not tested immediately were stored in a silica gel desiccator. The surface exposed to the work environment was 1 cm².

2.3. Theoretical Considerations

According to the mixed potential theory [45], any electrochemical reaction can be divided into two or more oxidation and reduction reactions, without accumulating electric

charges during the reactions. In a corrodible system, oxidation of the metal (corrosion) and reduction of certain elements in the solution occurs at the same rate and the net current measured is zero [46–48].

$$i_{meas} = i_{red} - i_{ox} = 0 \quad (1)$$

i_{meas} is the measured net current,

i_{red} is the reduction current (rate at which electrons are gained by elements in the solution),

i_{ox} is the oxidation current (rate at which electrons are lost by the metal).

When a metal or alloy is placed in contact with a solution, the metal will assume a potential that is dependent on the nature of the material and the nature of the solution. This open circuit potential, without the application of any potential from outside the cell, is the corrosion potential E_{cor} .

Many of the modern corrosion techniques are based on the theoretical analysis of the shapes of the Stern and Geary polarization curves.

If a potential is imposed on the material from an external source and the reaction rate is controlled, it results:

$$i_{red} = i_{ex(red)} e^{-\eta/\beta_1} \quad (2)$$

and

$$i_{ox} = i_{ex(ox)} e^{-\eta/\beta_2} \quad (3)$$

where: $i_{ex(red)}$ is the exchange reduction current, $i_{ex(ox)}$ is the exchange oxidation current, η is the overvoltage, being equal to the difference between the potential imposed from the material outside, E_{appl} and corrosion potential, E_{cor} ;

β_1 and β_2 —Tafel constants.

By logarithming the Equations (2) and (3), we obtain the equations of J. Tafel:

$$\left. \begin{aligned} \eta &= -\beta_C \cdot \log\left(\frac{i_{red}}{i_{ex}}\right) \\ \eta &= -\beta_A \cdot \log\left(\frac{i_{red}}{i_{ex}}\right) \end{aligned} \right\} \quad (4)$$

where $\beta_C = 2.3 \cdot \beta_1$ and $\beta_A = 2.3 \cdot \beta_2$ being called Tafel's constants, cathodic and anodic respectively [21].

Once the potential E_{cor} and the corrosion current i_{cor} are determined, the corrosion rate can be calculated.

According to Faraday's law:

$$Q = nFW/M \quad (5)$$

where Q —Coulomb;

n —the number of electrons involved in electrochemical reactions;

F —Faraday's constant, 96,487 Coulombs;

W —the lost weight of the material.

M —the atomic mass of the material.

It can be written:

$$W/t = i_{cor}(E.W.)/F \quad (6)$$

where $W/t = C.R.$ —corrosion rate in g/s;

$E.W. = M/n$ —equivalent weight, n —the number of electrons involved in the reaction.

Because C.R. it is usually expressed in units of length/time (mm/year or milliinch/year-mpy) we have [49]:

$$C.R. = 0.13 i_{cor} (E.W.)/\rho, [\text{mpy}] \quad (7)$$

where, ρ is material density, g/cm³;

i_{cor} —corrosion current density, $\mu\text{A}/\text{cm}^2$.

3. Results and Discussion

3.1. Testing of Materials Used for Mixing Blades (in Cement Paste)

Figure 4 shows for exemplification the polarization curve for F1 material and Figure 5 shows the Tafel curves obtained after testing the samples made of cast-iron materials.

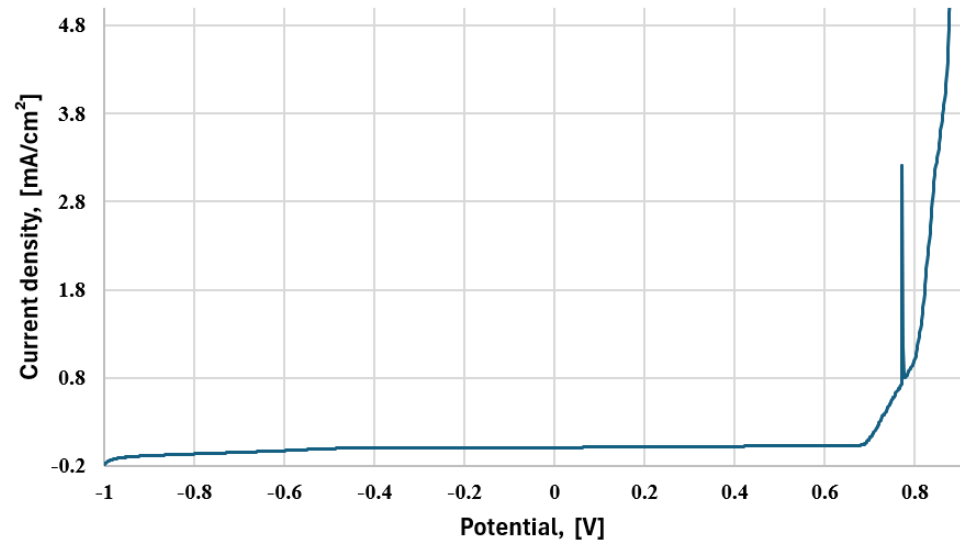


Figure 4. Polarization curve for F1 cast iron.

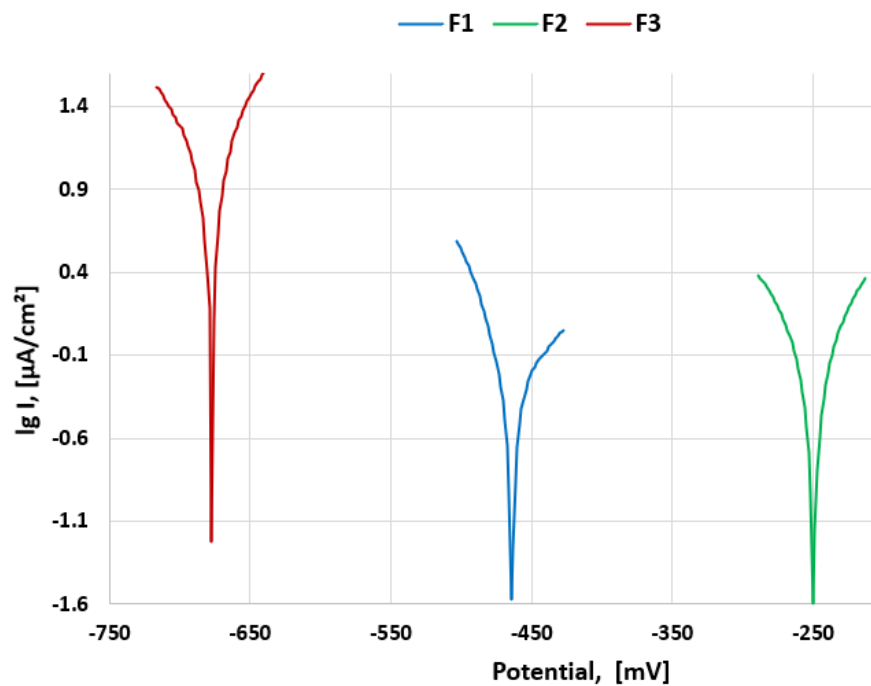
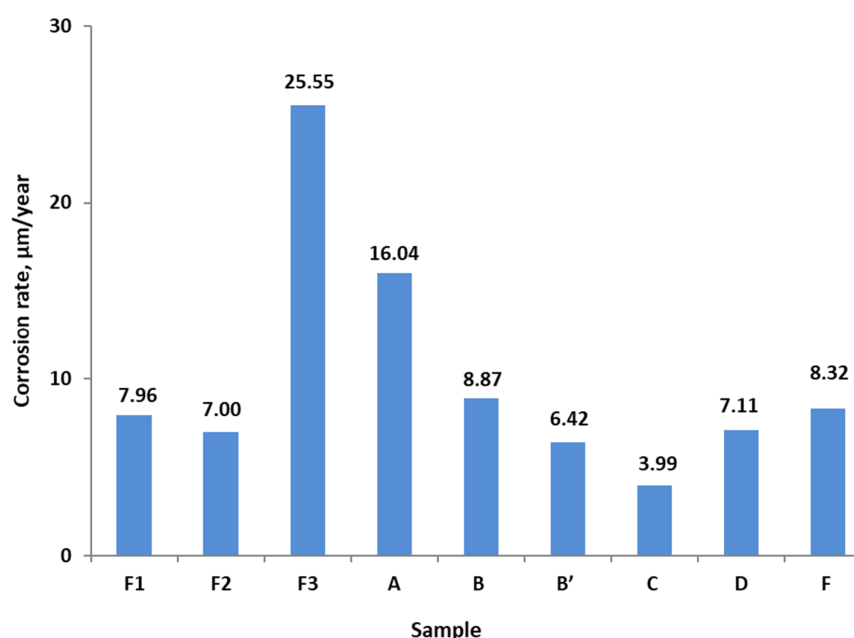


Figure 5. Tafel plots for cast iron samples.

The determined parameters for the samples tested in cement paste are presented in Table 5, and the comparison between corrosion rates in Figure 6.

Table 5. The parameters determined for samples tested in cement paste.

Sample	Parameter				
	i_{corr} , $\mu\text{A}/\text{cm}^2$	E_{corr} , mV	β_A , mV	β_C , mV	CR, $\mu\text{m}/\text{year}$
F1	0.685	−383.1	55.7	−56.8	7.96
F2	0.603	−249.6	57.2	−63.4	7.00
F3	2.198	−439	62.1	−60	25.55
A	1.3804	−449.3	57.3	−65.3	16.04
B	0.7639	−468	85	−38	8.87
B' (cement paste)	0.5525	−565.7	18.3	−41.9	6.42
C	0.3442	−325.7	43.3	−37.9	3.99
D (cement paste)	0.6121	−504.2	25.3	−86	7.11
F (cement paste)	0.7167	−500	58.3	−55	8.32

**Figure 6.** Corrosion rate determined for the samples tested in cement paste.

The corrosion current density i_{corr} represents the rate at which corrosion occurs. Higher values indicate a higher rate of corrosion. The corrosion potential E_{cor} represents the thermodynamic tendency for corrosion to occur. More negative values indicate a higher tendency for corrosion. F3 has the most negative corrosion potential, suggesting it is the most susceptible to corrosion among the three samples. The anodic Tafel slope β_A reflects the rate of anodic dissolution during corrosion. Higher values suggest a higher rate of anodic dissolution. F3 shows the highest value, indicating a potentially higher rate of anodic dissolution compared to F1 and F2. The cathodic Tafel slope β_C reflects the rate of cathodic reduction during corrosion. F2 shows the most negative value, suggesting potentially faster cathodic reduction compared to F1 and F3. This observation can be correlated with the values of corrosion rate, observing that F3 present the highest corrosion rate, 3.2 and 3.6 times greater than F1 and F2 respectively. This conclusion is in accordance with the previous work of the authors [16] where the same materials were used for tribological tests in different environments (mixture of mineral aggregate, sand, cement, and water), using Baroid tribometer and it was found that the cast iron with 9% Cr had the lowest abrasive wear resistance in all testing environments. Also, in another investigation performed by the

authors [18] it was concluded that blade made of F2 material had the smallest corrosion rate compared to blades made from F1 and F3 cast iron, and therefore the best wear resistance for all values of blade inclination angle.

Among the steel samples, sample C shows the lowest corrosion rate (3.99 $\mu\text{m}/\text{year}$), indicating that it has the best corrosion resistance in cement paste, while sample A has the highest corrosion rate (16.04 $\mu\text{m}/\text{year}$).

Generally, steel samples exhibit a wide range of corrosion rates [50] (from 3.99 $\mu\text{m}/\text{year}$ to 16.04 $\mu\text{m}/\text{year}$), with some (B', C and D) performing better than cast iron.

3.2. Testing of Materials Used for Rotary Dryers (in Water)

In Table 6 are presented the parameters obtained from the experimental tests (in water environment) for the steels used in manufacturing of rotary dryers.

Table 6. The parameters determined for samples tested in water.

Sample	Parameter				
	i_{corr} , $\mu\text{A}/\text{cm}^2$	E_{corr} , mV	β_A , mV	β_C , mV	CR, $\mu\text{m}/\text{Year}$
B	4.1307	−111.1	48.4	−96.8	48.00
B' (water)	0.7942	−378.3	58.7	−53	9.23
D (water)	4.8271	−521.1	45.4	−59	56.1
E	5.9076	−527.5	36.6	−58.3	68.65
F (water)	4.9443	−567.3	40.4	−55.7	57.46
G	4.8157	−576.4	43.5	−64.4	55.96
S	2.1827	−205.9	45.5	−58.9	25.36

The corrosion rates vary significantly across different materials (see Figure 7). For example, sample E exhibits the highest corrosion rate (68.65 $\mu\text{m}/\text{year}$), while sample B' shows the lowest corrosion rates (9.23 $\mu\text{m}/\text{year}$). Therefore, for the flights of rotary dryers used to dry mineral aggregates, sample B' is the most suitable due to its good corrosion resistance. Samples E, D, F, and G are not recommended due to their high corrosion rates, while samples B and S offer moderate performance. Also, it was found that substituting steel S (S235) with steel B' (P265GH) can decrease the corrosion rate by nearly 65% due to several key differences in their chemical compositions. P265GH has a significantly lower carbon content (0.072% vs. 0.171%), which reduces carbide formation that can deplete protective chromium. It also has lower manganese (0.51% vs. 1.37%), minimizing the formation of less protective manganese oxides. Additionally, P265GH contains higher levels of chromium (0.12% vs. 0.0279%), nickel (0.09% vs. 0.0205%), and copper (0.08% vs. negligible), which enhance the formation and stability of a protective oxide film on the steel surface. This oxide film acts as a barrier against corrosive elements in water, significantly improving corrosion resistance. Thus, the optimized alloying elements in P265GH result in a much lower corrosion rate compared to S235 when exposed to water.

Comparing the data from Figures 6 and 7, it can be observed that corrosion rates also vary depending on the testing environment. Materials tested in water generally exhibit higher corrosion rates compared to those tested in cement paste. For instance, material B shows a corrosion rate of 48 $\mu\text{m}/\text{year}$ in water, significantly higher (5.41 times) than its corrosion rate of 8.87 $\mu\text{m}/\text{year}$ in cement paste. Steel B' revealed 1.43 times higher corrosion rate in water compared with cement paste, while steel F presents very big differences between water and cement paste environment (corrosion rate is 6.9 times greater in water).

This observation highlights the importance of considering the environment in which materials will be used, as different environments can accelerate corrosion processes.

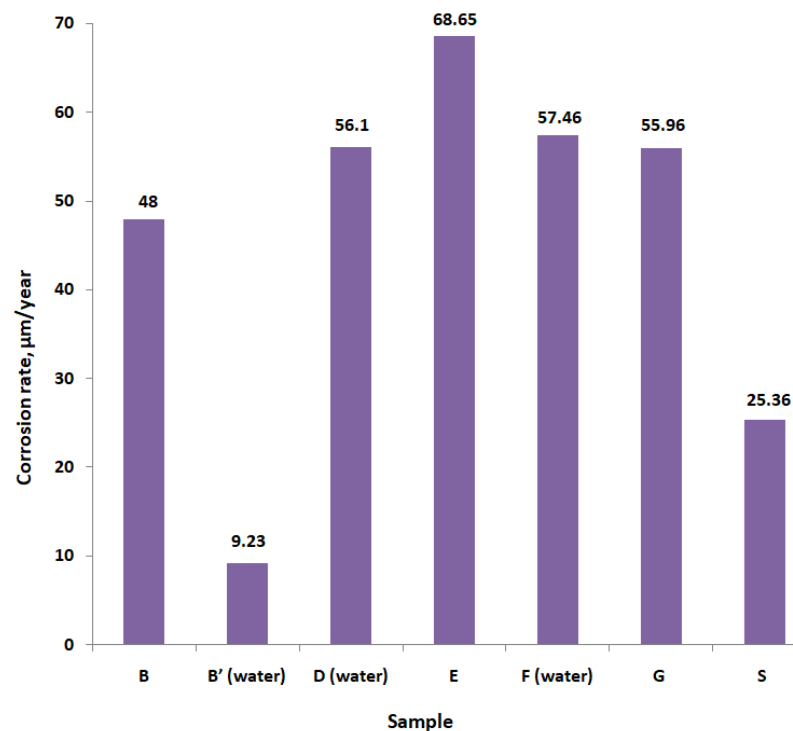


Figure 7. The values of corrosion rate determined for the samples tested in water.

4. Conclusions

Industrial applications specific to concrete industry present challenges in the choice of metallic materials. The appropriate choice of materials leads to an increase in the operating life of equipment and cost reduction.

The corrosion rate data provides valuable guidance for material selection in various applications. Materials with lower corrosion rates are preferable for environments where corrosion is a concern, as they offer greater durability and longer service life. Understanding the corrosion behavior of different materials in specific environments allows engineers and designers to make informed decisions when selecting materials for construction, infrastructure, and industrial applications.

The research results presented in this paper demonstrate that, in some applications, material testing can provide economical solutions for equipment components in the concrete industry. Proposals to replace cast irons, used in the manufacture of concrete mixing blades, with steels are justified in specific situations: corrective/accidental maintenance works; situations involving the reduction of spare parts costs; use the equipment for a short time. It is observed that, in such cases, steels of type B' and C offer—from the point of view of corrosion resistance—similar results to cast iron.

Similarly, for use in mineral aggregate driers, judicious choice of steels can lead to considerable reductions in operating costs (including maintenance) and increased equipment durability. The results obtained by the authors show that it is beneficial to replace steel S with steel B', reducing the corrosion rate by almost 65%.

For a correct decision, the results of corrosion tests (as presented in this article) must be combined with the results of wear tests [1,18], specific to the operation of the studied equipment. In this way, pertinent and complete conclusions can be drawn regarding the choice of technological solutions.

Further research could explore the underlying factors contributing to the observed differences in corrosion rates across materials and environments.

Investigating the microstructure, composition, and surface characteristics of the materials could provide insights into their corrosion resistance mechanisms and help optimize material properties for enhanced performance.

Author Contributions: Conceptualization, R.G.R. and M.G.P.; methodology, R.G.R. and M.G.P.; validation, R.G.R. and M.G.P.; formal analysis, M.G.P.; investigation, R.G.R., M.G.P., E.L., M.T., A.N. and A.B.; resources, A.N. and A.B.; writing—original draft preparation, E.L. and M.T.; writing—review and editing, M.T.; visualization R.G.R. and M.G.P.; supervision, M.G.P. All authors have read and agreed to the published version of the manuscript.

Funding: This research received no external funding.

Institutional Review Board Statement: Not applicable.

Informed Consent Statement: Not applicable.

Data Availability Statement: Data are contained within the article.

Conflicts of Interest: The authors declare no conflicts of interest.

References

- Burlacu, A.; Gabriel Petrescu, M.; George Ripeanu, R.; Dumitru, T.; Victor Laudacescu, E.; Naim Ramadana, I.; Niță, A. Experimental Investigations on Wear Phenomena Specific to Rotary Dryer Flights (Blades). *Tribol. Ind.* **2024**, *46*, 56–65. [[CrossRef](#)]
- Revol, D.; Briens, C.L.; Chabagno, J.M. The Design of Flights in Rotary Dryers. *Powder Technol.* **2001**, *121*, 230–238. [[CrossRef](#)]
- Ghasemi, A.; Hasankhoei, A.; Parsapour, G.; Razi, E.; Banisi, S. A Combined Physical and DEM Modelling Approach to Improve Performance of Rotary Dryers by Modifying Flights Design. *Dry. Technol.* **2021**, *39*, 548–565. [[CrossRef](#)]
- Karali, M.A.; Specht, E.; Herz, F.; Mellmann, J.; Refaey, H.A. Unloading Characteristics of Flights in a Flighted Rotary Drum Operated at Optimum Loading. *Powder Technol.* **2018**, *333*, 347–352. [[CrossRef](#)]
- Nascimento, S.M.; Santos, D.A.; Barrozo, M.A.S.; Duarte, C.R. Solids Holdup in Flighted Rotating Drums: An Experimental and Simulation Study. *Powder Technol.* **2015**, *280*, 18–25. [[CrossRef](#)]
- Karali, M.A.; Sunkara, K.R.; Herz, F.; Specht, E. Experimental Analysis of a Flighted Rotary Drum to Assess the Optimum Loading. *Chem. Eng. Sci.* **2015**, *138*, 772–779. [[CrossRef](#)]
- Silveira, J.C.; Lima, R.M.; Brandao, R.J.; Duarte, C.R.; Barrozo, M.A.S. A Study of the Design and Arrangement of Flights in a Rotary Drum. *Powder Technol.* **2022**, *395*, 195–206. [[CrossRef](#)]
- Ilhan, E.; Findik, F.; Aslanlar, S. An Investigation of the Factors Affecting the Design of Drum Dryers. *Mater. Des.* **2003**, *24*, 503–507. [[CrossRef](#)]
- Fasano, J.; Janz, E.E.; Myers, K. Design Mixers to Minimize Effects of Erosion and Corrosion Erosion. *Int. J. Chem. Eng.* **2012**, *2012*, 1–8. [[CrossRef](#)]
- Yao, Z.; Yang, R.; Yuan, W.; An, H. Mechanical analysis and optimal design of mixing paddles for sam Mixers. *Acad. J. Manuf. Eng.* **2019**, *17*, 80–86.
- Khidir, T.C. Designing, Remodeling and Analyzing the Blades of Portable Concrete Mixture. *Int. J. Mech. Eng. Robot. Res.* **2018**, *7*, 674–678. [[CrossRef](#)]
- Jungedal, M. Mild Impact Wear in a Concrete Mixer, an Evaluation of Wet Abrasive Wear. Master's Thesis, Royal Institute of Technology Department of Material Science and Engineering SE-100 44, Stockholm, Sweden, 2012.
- Zhang, H.; Feng, P.; Ying, W. Abrasive Wear and Optimal Installation Angle of Concrete Double-Horizontal Shaft Mixer Stirring Blades. *SN Appl. Sci.* **2020**, *2*, 1067. [[CrossRef](#)]
- Valigi, M.C.; Logozzo, S.; Rinchi, M. Wear Resistance of Blades in Planetary Concrete Mixers. Part II: 3D Validation of a New Mixing Blade Design and Efficiency Evaluation. *Tribol. Int.* **2016**, *103*, 37–44. [[CrossRef](#)]
- Valigi, M.C.; Logozzo, S.; Rinchi, M. Wear Resistance of Blades in Planetary Concrete Mixers. Design of a New Improved Blade Shape and 2D Validation. *Tribol. Int.* **2016**, *96*, 191–201. [[CrossRef](#)]
- Niță, A.; Petrescu, M.G.; Dumitru, T.; Burlacu, A.; Tănase, M.; Laudacescu, E.; Ramadan, I. Experimental Research on the Wear Behavior of Materials Used in the Manufacture of Components for Cement Concrete Mixers. *Materials* **2023**, *16*, 2326. [[CrossRef](#)]
- Labiapari, W.S.; Gonçalves, R.J.; De Alcântara, C.M.; Pagani, V.; Di Cunto, J.C.; De Mello, J.D.B. Understanding Abrasion-Corrosion to Improve Concrete Mixer Drum Performance: A Laboratory and Field Approach. *Wear* **2021**, *477*, 203830. [[CrossRef](#)]
- Niță, A.; Laudacescu, E.; Petrescu, M.G.; Dumitru, T.; Burlacu, A.; Bădoiu, D.G.; Tănase, M. Experimental Research Regarding the Effect of Mineral Aggregates on the Wear of Mixing Blades of Concrete Mixers. *Materials* **2023**, *16*, 5047. [[CrossRef](#)] [[PubMed](#)]
- Soleymani, H.R.; Ismail, M.E. Comparing Corrosion Measurement Methods to Assess the Corrosion Activity of Laboratory OPC and HPC Concrete Specimens. *Cem. Concr. Res.* **2004**, *34*, 2037–2044. [[CrossRef](#)]
- Garcia, E.; Torres, J.; Rebolledo, N.; Arrabal, R.; Sanchez, J. Corrosion of Steel Rebars in Anoxic Environments. Part I: Electrochemical Measurements. *Materials* **2021**, *14*, 2491. [[CrossRef](#)]
- Elsener, B. Corrosion Rate of Steel in Concrete—Measurements beyond the Tafel Law. *Corros. Sci.* **2005**, *47*, 3019–3033. [[CrossRef](#)]
- Sanusi, M.S.; Shamsudin, S.R.; Rahmat, A.; Wardan, R. *Electrochemical Corrosion Behaviours of AISI 304 Austenitic Stainless Steel in NaCl Solutions at Different pH*; AIP Publishing: Ho Chi Minh, Vietnam, 2018; p. 020116.
- Fahim, A.; Dean, A.E.; Thomas, M.D.A.; Moffatt, E.G. Corrosion Resistance of Chromium-steel and Stainless Steel Reinforcement in Concrete. *Mater. Corros.* **2019**, *70*, 328–344. [[CrossRef](#)]

24. Andrade, C.; Alonso, C. Test Methods for On-Site Corrosion Rate Measurement of Steel Reinforcement in Concrete by Means of the Polarization Resistance Method. *Mat. Struct.* **2004**, *37*, 623–643. [[CrossRef](#)]
25. Dubuc, B.; Ebrahimkhanlou, A.; Salamone, S. Corrosion Monitoring of Prestressed Concrete Structures by Using Topological Analysis of Acoustic Emission Data. *Smart Mater. Struct.* **2019**, *28*, 055001. [[CrossRef](#)]
26. Ming, J.; Shi, J. Distribution of Corrosion Products at the Steel-Concrete Interface: Influence of Mill Scale Properties, Reinforcing Steel Type and Corrosion Inducing Method. *Constr. Build. Mater.* **2019**, *229*, 116854. [[CrossRef](#)]
27. Chang, Z.-T.; Cherry, B.; Marosszeky, M. Polarisation Behaviour of Steel Bar Samples in Concrete in Seawater. Part 2: A Polarisation Model for Corrosion Evaluation of Steel in Concrete. *Corros. Sci.* **2008**, *50*, 3078–3086. [[CrossRef](#)]
28. Otieno, M.; Ikotun, J.; Ballim, Y. Experimental Investigations on the Influence of Cover Depth and Concrete Quality on Time to Cover Cracking Due to Carbonation-Induced Corrosion of Steel in RC Structures in an Urban, Inland Environment. *Constr. Build. Mater.* **2019**, *198*, 172–181. [[CrossRef](#)]
29. Lambert, P.; Page, C.L.; Vassie, P.R.W. Investigations of Reinforcement Corrosion. 2. Electrochemical Monitoring of Steel in Chloride-Contaminated Concrete. *Mater. Struct.* **1991**, *24*, 351–358. [[CrossRef](#)]
30. González, J.A.; Miranda, J.M.; Feliu, S. Considerations on Reproducibility of Potential and Corrosion Rate Measurements in Reinforced Concrete. *Corros. Sci.* **2004**, *46*, 2467–2485. [[CrossRef](#)]
31. Meng, D.; Lin, S.; Azari, H. Nondestructive Corrosion Evaluation of Reinforced Concrete Bridge Decks with Overlays: An Experimental Study. *J. Test. Eval.* **2020**, *48*, 516–537. [[CrossRef](#)]
32. Gulikers, J. Statistical Interpretation of Results of Potential Mapping on Reinforced Concrete Structures. *Eur. J. Environ. Civ. Eng.* **2010**, *14*, 441–466. [[CrossRef](#)]
33. Valipour, M.; Shekarchi, M.; Ghods, P. Comparative Studies of Experimental and Numerical Techniques in Measurement of Corrosion Rate and Time-to-Corrosion-Initiation of Rebar in Concrete in Marine Environments. *Cem. Concr. Compos.* **2014**, *48*, 98–107. [[CrossRef](#)]
34. Ghods, P.; Isgor, O.B.; Pour-Ghaz, M. A Practical Method for Calculating the Corrosion Rate of Uniformly Depassivated Reinforcing Bars in Concrete. *Mater. Corros.* **2007**, *58*, 265–272. [[CrossRef](#)]
35. Zou, Z.H.; Wu, J.; Wang, Z.; Wang, Z. Relationship between Half-Cell Potential and Corrosion Level of Rebar in Concrete. *Corros. Eng. Sci. Technol.* **2016**, *51*, 588–595. [[CrossRef](#)]
36. Li, C.; Chen, Q.; Wang, R.; Wu, M.; Jiang, Z. Corrosion Assessment of Reinforced Concrete Structures Exposed to Chloride Environments in Underground Tunnels: Theoretical Insights and Practical Data Interpretations. *Cem. Concr. Compos.* **2020**, *112*, 103652. [[CrossRef](#)]
37. ASTM G5-94; Standard Reference Test Method for Making Potentiostatic and Potentiodynamic Anodic Polarization Measurements. ASTM International: West Conshohocken, PA, USA, 2011.
38. ASTM G1-90; Standard Practice for Preparing, Cleaning, and Evaluating Corrosion Test Specimens. ASTM: West Conshohocken, PA, USA, 1999.
39. EN 10028-2:2003; Flat Products Made of Steels for Pressure Purposes—Part 2: Non-Alloy and Alloy Steels with Specified Elevated Temperature Properties. European Committee for Standardization: Brussels, Belgium, 2003.
40. ASME SA-516; Specification for Pressure Vessel Plates, Carbon Steel, for Moderate- and Lower Temperature Service. ASTM International: New York, NY, USA, 2017.
41. EN 10088-2:2005; Stainless Steels—Part 2: Technical Delivery Conditions for Sheet/Plate and Strip of Corrosion Resisting Steels for General Purposes. European Committee for Standardization: Brussels, Belgium, 2005.
42. ASTM A29/A29M-23; Standard Specification for General Requirements for Steel Bars, Carbon and Alloy, Hot-Wrought. ASTM International: West Conshohocken, PA, USA, 2023.
43. EN 10083; Steels for Quenching and Tempering. European Committee for Standardization: Brussels, Belgium, 2006.
44. EN 10025; Hot Rolled Products of Structural Steels. European Committee for Standardization: Brussels, Belgium, 2019.
45. Mansfeld, F. Simultaneous Determination of Instantaneous Corrosion Rates and Tafel Slopes from Polarization Resistance Measurements. *J. Electrochem. Soc.* **1973**, *120*, 515. [[CrossRef](#)]
46. von Baekmann, W.; Schwenk, W.; Prinz, W.; von Baekmann, W. (Eds.) *Handbook of Cathodic Corrosion Protection: Theory and Practice of Electrochemical Protection Processes*, 3rd ed.; Gulf Professional Publishing: Houston, TX, USA, 1997; ISBN 978-0-88415-056-5.
47. Ripeanu, R.G.; Ispas, V.; Ispas, D. Austenitic Stainless Steel Type AISI 316L Corrosive Behavior in Hair Shampoo Medium. *J. Balk. Tribol. Assoc.* **2012**, *18*, 36–43.
48. Dudu, C.; Drumeanu, A.C.; Ripeanu, R.G.; Dinita, A. Some Considerations Regarding the Influence of Working Conditions on the Corrosion Wear of the Injection Water Treatment Plant Equipment. *IOP Conf. Ser. Mater. Sci. Eng.* **2020**, *724*, 012033. [[CrossRef](#)]
49. Eškinja, M.; Moshtaghi, M.; Hönig, S.; Zehethofer, G.; Mori, G. Investigation of the Effects of Temperature and Exposure Time on the Corrosion Behavior of a Ferritic Steel in CO₂ Environment Using the Optimized Linear Polarization Resistance Method. *Results Mater.* **2022**, *14*, 100282. [[CrossRef](#)]
50. Ahlström, J. Corrosion of Steel in Concrete at Various Moisture and Chloride Levels. Ph.D. Thesis, Division of Building Materials. LTH, Lund University, Lund, Sweden, 2014.

Disclaimer/Publisher’s Note: The statements, opinions and data contained in all publications are solely those of the individual author(s) and contributor(s) and not of MDPI and/or the editor(s). MDPI and/or the editor(s) disclaim responsibility for any injury to people or property resulting from any ideas, methods, instructions or products referred to in the content.